Mitochondrial Ca^{2+} Uniporter haploinsufficiency enhances long-term potentiation at hippocampal mossy fibre synapses

Michael J. Devine[1,*], Blanka R. Szulc[1,*], Jack H. Howden[1,*],

Guillermo López-Doménech[1], Arnaud Ruiz[2] and Josef T. Kittler[1]

[1]Department of Neuroscience, Physiology and Pharmacology, University College London, Gower Street, London WC1E 6BT, UK

[2]Department of Pharmacology, School of Pharmacy, University College London, Brunswick Square, London WC1N 1AX, UK

*equal contribution

‡Corresponding authors

Josef T. Kittler, Department of Neuroscience, Physiology, and Pharmacology, University College London, Gower Street, London WC1E 6BT, UK.

Tel: + 44 207 679 3218, Fax: +44 207 916 7968, Email: j.kittler@ucl.ac.uk

Blanka R. Szulc, Department of Lifelong Learning, Global and Lifelong Learning, University of Kent, Medway Building, Medway, ME4 4AG, UK. Tel: + 44 1634 202010, Email : b.hilton@kent.ac.uk

Key words: Mitochondria; Calcium; MCU; Long-term potentiation; Mossy fibre synapse

Abstract

Long-term changes in synaptic strength form the basis of learning and memory. These changes rely upon energy demanding mechanisms which are regulated by local Ca^{2+} signaling. Mitochondria are optimised for providing energy and buffering Ca^{2+}. However, our understanding of the role of mitochondria in regulating synaptic plasticity is incomplete. Here we have used optical and electrophysiological techniques in cultured hippocampal neurons and *ex vivo* hippocampal slices from mice with haploinsufficiency of the mitochondrial Ca^{2+} uniporter ($MCU^{+/-}$) to address whether reducing mitochondrial Ca^{2+} uptake alters synaptic transmission and plasticity. We found that cultured $MCU^{+/-}$ hippocampal neurons have impaired Ca^{2+} clearance, and consequently enhanced synaptic vesicle fusion at presynapses occupied by mitochondria. Furthermore, long-term potentiation (LTP) at mossy fibre (MF) synapses, a process which is dependent on presynaptic Ca^{2+} accumulation, is enhanced in $MCU^{+/-}$ slices. Our results reveal a previously unrecognized role for mitochondria in regulating presynaptic plasticity of a major excitatory pathway involved in learning and memory.

Introduction

Mitochondria positioned at presynapses are an important source of ATP for powering synaptic transmission, but they also take up local Ca^{2+}, thereby modulating synaptic activity (Devine and Kittler, 2018). We and others have reported that presynaptic mitochondria reduce activity-dependent local Ca^{2+} transients, reducing neurotransmission (Kwon et al., 2016; Vaccaro et al., 2017). This is mediated by Ca^{2+} uptake via the mitochondrial calcium uniporter (MCU). MCU forms a Ca^{2+}-selective pore in the inner mitochondrial membrane enabling rapid Ca^{2+} uptake into the mitochondrial matrix (Patron et al., 2013). MICU1, MICU2 and MICU3 gate Ca^{2+} entry into the MCU, thereby setting the Ca^{2+} uptake threshold (Stefani et al., 2015). MICU1 and MICU2 require high local $[Ca^{2+}]$ for Ca^{2+} uptake (Kamer and Mootha, 2015). However, in neurons, MCU is gated by brain-specific MICU3, with a 10-fold

lower uptake threshold (Ashrafi et al., 2020). Thus neuronal mitochondria play a major role in Ca^{2+} homeostasis. Indeed, pharmacological MCU blockade demonstrates that presynaptic mitochondria account for ~40% of Ca^{2+} clearance in rat sensory neurons (Shutov et al., 2013).

Presynaptic Ca^{2+} signals are important in regulating synaptic plasticity. High-frequency tetanic stimulation enhances synaptic transmission over short timescales (minutes) via post-tetanic potentiation (PTP), which is thought to be mediated by sustained elevated presynaptic Ca^{2+} due to prolonged stimulation (Katz and Miledi, 1968). Over longer timescales (hours), tetanic stimulation can be followed by a sustained increase in synaptic transmission called long-term potentiation (LTP), thought to underly learning and memory (Bliss and Lømo, 1973). LTP is governed by presynaptic mechanisms at hippocampal mossy fibre (MF) synapses, connecting dentate gyrus (DG) granule cells with CA3 neurons. MF LTP depends upon presynaptic Ca^{2+} accumulation during sustained activity (Nicoll and Schmitz, 2005). Furthermore, giant MF presynapses are replete with up to 50 mitochondria per terminal (Rollenhagen et al., 2007), and they undergo dramatic changes in synaptic strength. Therefore, this is a perfect system for studying the impact of mitochondria on short- and long-term plasticity. Pharmacological inhibition of mitochondrial Ca^{2+} uptake blocks PTP at crayfish neuromuscular junction (Tang and Zucker, 1997), and reducing MCU expression impairs short-term synaptic plasticity in cortical neurons (Kwon et al., 2016). However, whether MCU-mediated Ca^{2+} uptake modulates other forms of plasticity, or plasticity at other synapses, is unknown.

Here we investigate how MCU shapes synaptic plasticity at hippocampal synapses in neuronal cultures and MF synapses in slices using gene-targeted MCU knockout in mouse. We show that MCU haploinsufficiency ($MCU^{+/-}$) reduces mitochondrial presynaptic Ca^{2+} clearance, increasing release probability, despite reduced ATP. Strikingly, presynaptic LTP is enhanced when MCU is reduced. This highlights the importance of MCU-mediated presynaptic Ca^{2+} uptake in regulating basal neurotransmission and presynaptic plasticity of a major hippocampal excitatory synapse.

Results and Discussion

MCU$^{+/-}$ reduces presynaptic mitochondrial Ca^{2+} clearance

We used MCU$^{+/-}$ animals because MCU KO is embryonic lethal on the C57BL/6 background (Murphy et al., 2014). We confirmed that MCU protein levels are reduced in MCU$^{+/-}$ animals compared to wildtype littermate controls, throughout the brain and in neuronal cultures (Fig. 1a & 1b). In MCU$^{+/-}$ animals, MICU3 was reduced in all brain areas examined and MICU1 was reduced in hippocampus and cortex, compared to controls (Supplementary Fig. 1a & 1b). There were no gross anatomical differences between MCU$^{+/-}$ and control neurons (Supplementary Fig. 2a-e).

We then live-imaged neurons with a mitochondrially-targeted Ca^{2+} reporter (mitoGCaMP5) (Fig. 1c). Mitochondrial Ca^{2+} uptake, in response to neuronal stimulation, was significantly lower in MCU$^{+/-}$ neurons compared to controls (Fig. 1d & 1e). We imaged presynaptic Ca^{2+} transients in response to stimulation using a presynaptically-targeted Ca^{2+} reporter (SyGCaMP5) (Fig. 1f). By cotransfecting neurons with a fluorescent mitochondrial reporter (MtDsRed), we compared Ca^{2+} transients at boutons occupied by mitochondria with unoccupied boutons. We confirmed that, in control neurons, boutons occupied by mitochondria exhibit lower Ca^{2+} transients than unoccupied boutons (Fig. 1g & 1h) (Vaccaro et al., 2017). In contrast, Ca^{2+} transients at boutons in MCU$^{+/-}$ neurons were not altered by mitochondria (Fig. 1i and 1j). Ca^{2+} transients in boutons without mitochondria were identical in MCU$^{+/-}$ and controls, confirming that altering MCU gene dosage specifically impacts mitochondrial Ca^{2+} uptake (Fig. 1k and 1l).

Overall, MCU$^{+/-}$ reduces mitochondrial Ca^{2+} uptake sufficiently to block the effect of mitochondria on presynaptic Ca^{2+}.

MCU$^{+/-}$ enhances synaptic vesicle fusion and alters activity-dependent redistribution of mitochondria

To image synaptic vesicle (SV) fusion we used vGlut1pHluorin, whilst simultaneously imaging mitochondria with mitochondrially-targeted LSS-mKate2 (Fig. 2a). In controls, SV fusion was reduced at boutons occupied by

mitochondria (Fig. 2b and 2c). In contrast, presynaptic mitochondria in MCU^{+/-} neurons failed to alter SV fusion (Fig. 2d and 2e). Therefore, MCU^{+/-} blocks mitochondria from reducing Ca^{2+} clearance and consequent SV fusion at presynapses. MCU knockdown reportedly accelerates SV endocytosis by reducing mitochondrial Ca^{2+} efflux following neuronal stimulation, thereby lifting the breaking effect of Ca^{2+} on SV endocytosis (Marland et al., 2016). In agreement, we found accelerated SV endocytosis in MCU^{+/-} neurons compared to controls (Supplementary Fig. 3).

To exclude the possibility that MCU^{+/-} enhances SV fusion by enhancing ATP availability, we used PercevalHR (Tantama et al., 2013) to compare ATP in MCU^{+/-} neurons and controls following neuronal stimulation. ATP was lower in MCU^{+/-} (Supplementary Fig. 4a-d) consistent with the requirement for mitochondrial Ca^{2+} uptake to drive ATP production (Ashrafi et al., 2020).

Mitochondria redistribute to and from presynapses in response to prolonged (48 h) alterations in network activity, contributing to homeostatic plasticity (Vaccaro et al., 2017). We examined the impact of MCU^{+/-} on this redistribution by co-transfecting neurons with synaptophysin-GFP to label presynapses, and mitoDsRed to label mitochondria. We determined presynaptic mitochondrial occupancy in control and MCU^{+/-} neurons at baseline, and following 48 h treatment with tetrodotoxin (decreasing network activity) or picrotoxin (increasing network activity). In control (Fig. 2f & 2g) and MCU^{+/-} neurons (Fig. 2h & 2i), lowering activity reduced presynaptic mitochondrial occupancy. However, increasing activity failed to recruit mitochondria to presynapses in MCU^{+/-} neurons, in contrast to controls (Fig. 2i). Following picrotoxin, presynaptic mitochondrial occupancy in MCU^{+/-} neurons was significantly lower than in controls (two-tailed unpaired t-test, P = 0.0271), suggesting that MCU-mediated Ca^{2+} uptake is required for mitochondrial recruitment to presynapses. This is consistent with previous work demonstrating that increasing mitochondrial matrix Ca^{2+} ceases mitochondrial movement (Chang et al., 2011).

Increased mossy fibre excitability and enhanced presynaptic LTP in MCU$^{+/-}$ mice

Next, given that hippocampal MF boutons are replete with mitochondria, and that plasticity at these synapses is expressed presynaptically, we asked if MCU$^{+/-}$ changes synaptic plasticity at MF synapses. We examined basal synaptic transmission by plotting the slope (output) of evoked fEPSP in response to increasing stimulation intensity (input). Input-output curves from MCU$^{+/-}$ slices were similar to WT littermate controls (Fig. 3a & 3b). We observed higher fibre volley amplitudes in MCU$^{+/-}$ at all but the weakest stimulus strengths (Fig. 3c), suggesting increased presynaptic strength. We then compared fEPSP slope against fibre volley amplitude. MCU$^{+/-}$ exhibited higher amplitude fibre volleys for equivalent fEPSP slope values compared to controls (Fig.3d). These results suggest that DG-CA3 transmission is increased in MCU$^{+/-}$.

Paired-pulse facilitation (a form of presynaptic short-term plasticity) is large at MF synapses (Salin et al., 1996). It is assessed by induction of two closely spaced stimuli. The characteristic paired-pulse facilitation of DG-evoked EPSPs in control slices was absent in MCU$^{+/-}$, at intervals less than 200ms (Fig. 3f). As paired-pulse ratio inversely correlates with release probability, and is attributed to presynaptic Ca^{2+}, this result is consistent with enhanced release probability in MCU$^{+/-}$ at shorter intervals (20-100ms).

Finally, we examined the role of MCU$^{+/-}$ on LTP elicited by long high-frequency stimulation delivered to stratum granulosum. PTP (resulting from slow efflux of accumulated mitochondrial Ca^{2+} (Lee et al., 2007; Tang and Zucker, 1997)), was increased in MCU$^{+/-}$ compared to controls (Fig. 3g,h). Moreover, LTP in MCU$^{+/-}$ was greater than in controls (Fig. 3g,i). DCG-IV (1 µM) had a depressant effect, consistent with the high sensitivity of MFs to group II metabotropic glutamate receptor agonists, confirming that measured LTP was specific to MF synapses.

Our results show that presynaptic mitochondrial Ca^{2+} uptake via MCU limits both SV fusion and endocytosis, and LTP, despite increasing ATP. We predict that the observed increase in MF LTP in MCU$^{+/-}$ would correlate with

enhanced learning and memory. Albeit a different form of LTP, increasing hippocampal NMDA receptor activity enhances neurotransmission and LTP at Schaffer-CA1 synapses, with improved learning and memory in mice (Tang et al., 1999). Furthermore, pharmacological inhibition of DG-CA3 transmission impairs spatial learning in mice (Lassalle et al., 2000).

Mitochondria sense changes in cytoplasmic Ca^{2+} and energy usage which are both indicators of neuronal activity, and presynaptic mitochondria can alter synaptic activity via MCU-mediated Ca^{2+} uptake (Kwon et al., 2016; Vaccaro et al., 2017). This ability to both detect and change neuronal activity suggests that mitochondria could regulate neuronal network activity (Ruggiero et al., 2021). Mitochondria have been shown to regulate network activity of hippocampal neurons, specifically the mean firing rate set point (Styr et al., 2019). Our data suggest that mitochondria also regulate the set point of mossy fibre LTP.

That MCU sets MF LTP at a submaximal level might help protect MF synapses from excitotoxicity. By analogy, NMDA receptor levels are downregulated at postsynapses in the adult brain (Bai et al., 2004; Law et al., 2003), which potentially protect Schaffer-CA1 synapses from excitotoxicity by limiting Ca^{2+} flux through NMDA receptors. However, aged mice with NMDA receptor overexpression maintain enhanced learning and memory performance (Cao et al., 2007), suggesting that long-term enhancement of LTP is not necessarily deleterious. Mitochondria might reduce the LTP set point to conserve resources, because enhanced neurotransmission and LTP in $MCU^{+/-}$ mice is likely metabolically expensive. Mitochondria can meet the energy requirements of active synapses through ATP provision (Pathak et al., 2015; Rangaraju et al., 2014). Moreover, when glucose is limited, neuronal metabolism switches to oxidative phosphorylation using lactate or pyruvate as fuel, and active synapses need MCU-mediated Ca^{2+} uptake to drive ATP production under these conditions (Ashrafi et al., 2020). Therefore, in real-world conditions of constrained food—and therefore fuel—availability, mitochondria that avidly take up Ca^{2+} via MCU are important to maintain ATP delivery. Constrained neurotransmission and LTP might be a consequence of enabling this metabolic flexibility. The need to balance accurate

neurotransmission with fuel availability is highlighted by recent work showing that the neocortex saves energy during food scarcity by sacrificing coding precision (Padamsey et al., 2021).

In summary, presynaptic mitochondria are able to couple synaptic activity to fuel availability, and therefore limit presynaptic Ca^{2+} at active synapses. This could potentially avert catastrophic energy shortages in active synapses, and neuronal toxicity due to Ca^{2+} overload.

Methods

Animal models

The mouse line $Mcu^{tm1b(EUCOMM)Hmgu}$ was obtained from MRC Harwell. MCU homozygous knockout animals are non-viable on this genetic background (C57BL/6), but heterozygous animals are viable and can breed. In contrast, MCU homozygous knockout animals on the outbred CD1 background are viable (Pan et al., 2013). Animals were maintained under controlled conditions (temperature 20 ± 2°C; 12 h light-dark cycle). Food and water were provided ad libitum. All experimental procedures were carried out in accordance with institutional animal welfare guidelines and licensed by the UK Home Office in accordance with the Animals (Scientific Procedures) Act 1986. All data involving procedures carried out in animals are reported in compliance with ARRIVE guidelines (Kilkenny et al., 2010).

Neuronal cultures and transfection

Primary hippocampal cultures were prepared as previously described from E16 mice of either gender (Vaccaro et al., 2017). Following 15 min treatment with 0.25% trypsin and trituration, cells were plated on poly-L-lysine coated round 12 mm coverslips for fixed experiments or 25 mm coverslips for live experiments at a density of 250,000 per 3 cm well. Neurons were transfected by lipofection with Lipofectamine 2000 at DIV 7 and then imaged at DIV 10-12.

Western blots

SDS-PAGE and Western blotting samples were denatured at 94 °C for 5 min in 3× SDS sample buffer (150 mM Tris, pH 8, 6% SDS, 0.3 M DTT, 0.3% bromophenol blue, and 30% glycerol). Polyacrylamide gels were prepared using 10% running gels and 5% stacking gels in Novex 1.5-mm cassettes and run using the Novex XCell SureLock Mini-Cell system. Gels were transferred onto Hybond-C nitrocellulose membrane (GE Healthcare). Membranes were blocked in 4% powder skimmed milk in TBS-T for 1–2 h. Antibodies were incubated in blocking solution (overnight at 4°C for primary antibodies or 1 h at RT for HRP-conjugated secondary antibodies). Membranes were developed using the ECL-Plus reagent (GE Healthcare) and acquired in a chemiluminescence imager coupled to a CCD camera (ImageQuant LAS 4000 mini). Densitometric analysis was performed using ImageJ software (https://imagej.nih.gov/ij/). Original blot images are shown in Supplementary Figs. 5 and 6.

Antibodies, DNA constructs and Reagents

SyGCaMP5, mitoDsRed, Synaptophysin-GFP, vGlut1pHluorin and Mito-LSSmKate2 have been previously described (Vaccaro et al., 2017). MitoGCaMP5 was obtained from Addgene (#58509; VV073: 1xCox8 - GCaMP5G in fubi). GW1-PercevalHR was a gift from Gary Yellen (Addgene plasmid # 49082; http://n2t.net/addgene:49082; RRID:Addgene_49082). MCU antibody was purchased from Atlas Antibodies (HPA016480) and used at 1:1000. Other antibodies used were: Anti-beta-Tubulin (Sigma T8328) at 1:2000, anti-MCUb (Abcepta AP12355b) at 1:500, anti-MCUR1 (Aviva ARP44777_P050) at 1:500, anti-MICU1 (Atlas HPA037480) at 1:500, anti-MICU2 (Abcam AB101465) at 1:500, anti-MICU3 (Atlas HPA024771) at 1:500, anti-NCLX (Abcam AB83551) at 1:500, anti-LETM1 (Atlas HPA011029) at 1:500, anti-VDAC1 (NeuroMab 75-204) at 1:1000. Picrotoxin (PTX) was purchased from Sigma Aldrich and used at 100 μM, Tetrodotoxin (TTX) was purchased from Tocris Bioscience and used at 1 μM.

Fixed imaging

After fixation using 4% PFA for 5 min, cells were washed twice and blocked in PBS solution containing 10% Horse Serum, 0.5% BSA and 0.2% Triton. Images of fixed cultures were taken on a Zeiss LSM700 confocal using a 63x oil objective (NA 1.4) and a 20x water objective (NA 1.0).

Live imaging

For measurement of Ca^{2+} and synaptic vesicle fusion, experiments were performed at 37°C whilst perfusing the coverslips in external solution containing 125 mM NaCl, 10 mM D-glucose, 10 mM HEPES, 5 mM KCl, 2 mM $CaCl_2$ and 1 mM $MgCl_2$, which was brought to a pH of 7.4 using NaOH. An inverted Zeiss Axiovert 200 microscope and a 63x oil objective (NA 1.4) coupled to a Photometrics Evolve camera were used to image frames with 30 ms exposure at 1 frame per second in the software Micro-Manager (Edelstein et al., 2010). Using Chroma filters, coverslips were excited through a D470/40X filter and emission was split using an Optosplit II (Cairn Research) (Awabdh et al., 2016) and a 565DCXR dichroic thereby collecting with HQ522/40M and HQ607/75M filters for SyGCaMP5 or VGlut1pHluorin and MtDsRed or Mito-LSSmKate2 respectively. Presynapses with and without mitochondria were discriminated on the basis of colocalisation of SyGCaMP5 or vGlut1pHluorin and MtDsRed or Mito-LSSmKate2 respectively: signal overlap for the duration of the imaging period was required for a synapse to be deemed occupied by a mitochondrion. Clear separation in signal was required to deem a synapse devoid of mitochondria. Field stimulation was achieved using a Grass S9 or S88 stimulator and a Warner Instruments stimulation bath. Individual stimulating pulses lasted for 1 ms and were set at 10 V as part of stimulation trains at 10 Hz, with durations of 10 s or 20 s.

For ATP measurements, primary hippocampal neurons were transfected with the ratiometric ATP:ADP sensor PercevalHR (Tantama et al., 2013) at DIV10 using Lipofectamine 2000. After 72 hours, imaging of neurons was performed using a Zeiss LSM700 confocal microscope with a 63x water immersion objective. PercevalHR was excited at 405 nm and at 488 nm, and

emission was collected at wavelengths longer than 510 nm. Images were acquired every 2 seconds for 200 seconds. Neurons were stimulated using 20 µM glutamate for 10 seconds at 30 seconds. ATP:ADP ratios over time were obtained in ImageJ by taking ROIs in each neuron, measuring average fluorescence in the ROIs for each channel and calculating the 488 nm/405 nm ratio. Mitochondrial Ca^{2+} uptake in response to glutamate stimulation was also measured by imaging MitoGCaMP5 using the confocal microscope, to verify that both glutamate stimulation and field stimulation produced an equivalent mitochondrial response. MitoGCaMP5G was excited at 488 nm and emission was collected at wavelengths longer than 510 nm. Images were acquired every 2 seconds for 200 seconds and neurons were stimulated using 20 µM glutamate for 10 seconds at 30 seconds. Mito-GCaMP5G fluorescence over time was obtained in ImageJ by taking ROIs in each neuron, measuring average fluorescence in the ROIs.

Field EPSP recordings

Transverse hippocampal slices (300 µm) were prepared from 5-8 week-old mice ($MCU^{+/-}$ males only, littermates) and obtained using a vibratome (Leica, VT-1200S). Brain was removed and kept in ice-cold dissecting solution. Slices were stored at 35°C for 30 min after slicing and then at 22°C. For the dissection and storage of slices, the solution contained (in mM): 87 NaCl, 25 $NaHCO_3$, 10 glucose, 75 sucrose, 2.5 KCl, 1.25 NaH_2PO_4, 0.5 $CaCl_2$ and 7 $MgCl_2$, saturated with 95% O_2/5% CO_2.

During experiments, slices were superfused with artificial cerebrospinal fluid solution (ACSF) containing: NaCl (125 mM), $NaHCO_3$ (25 mM), glucose (25 mM), KCl (2.5 mM), NaH_2PO_4 (1.25 mM), $CaCl_2$ (2 mM) and $MgCl_2$ (2 mM), equilibrated with 95% O_2/5% CO_2. The osmolarity and pH of perfusion solutions were adjusted to ~320 mOsmol/L and 7.3, respectively. All recordings were performed at room temperature (21-22 °C). A slice was transferred into the recording chamber and visualised with an Olympus BX 51WI microscope (Olympus Europa Holding GmbH, Hamburg, Germany) connected to a KPM-3 Hitachi infrared video camera. A bipolar stimulating

electrode (FHC Inc., Bowdoin, Maine, USA) was positioned under low magnification (10×) in the supra-granular blade of the dentate gyrus to activate mossy fibre synapses every 10 s using constant current (0.2-1 µA, 80 µs square pulses). A field recording electrode was placed in stratum lucidum in CA3. To set the intensity of stimulation, an input-output (I/O) relation was obtained for each slice when applying the control perfusion solution. The stimulus intensity was set such that the amplitude of the test fEPSP reached around 40% of maximum amplitude based on the I/O curve. Synaptic responses were recorded with an Axopatch 200B amplifier (Molecular Devices), filtered at 2 kHz (internal 4-pole low-pass Bessel filter), and sampled at 10 kHz. Two tests were routinely applied to verify that the signal recorded in stratum lucidum was a mossy fibre fEPSP. First, increasing the stimulation frequency caused pronounced facilitation (>2.5-fold at 1 Hz at room temperature) (Salin et al., 1996). Second, application of the group II mGluR agonist DCG-IV (1 µM) depressed the fEPSP amplitude to <20% of control fEPSP (Kamiya et al., 1996). Mossy fibre LTP was induced by long high-frequency tetanic stimulation (l-HFS) represented by 100 pulses in 1 s, 3 times, separated by 10 s. All LTP recordings were performed with the GABA$_A$ receptor antagonist bicuculline methiodide (10 µM), and NMDA receptor antagonist D-APV (25 µM) added to the ACSF to exclude any contribution from NMDA-dependent LTP.

Data analysis

Movies were aligned using the Cairn Image Splitter plugin in ImageJ. Graphs showing ΔF/F$_0$ were plotted using *Mathematica* (Wolfram Research). Regions of Interest were manually drawn and after background subtraction, fluorescence was normalised to the first 10 frames. Mean stimulation fluorescence was calculated as an average across a plateau equating to stimulation duration. For SV endocytosis, non-linear regression was used to fit a monoexponential function to the post-stimulation vGlutpHluorin data to derive the time constant (τ) of endocytosis. Exponentials were fitted between 1 – 60 s after termination of stimulation.

For co-localisation analysis, a region measuring 40 x 40 μm was chosen at least 300 μm from the soma. Co-localisation of Synaptophysin-GFP and MtDsRed was quantified as the fraction of Synaptophysin-GFP clusters which overlap with at least one MtDsRed-positive pixel. Images were thresholded in ImageJ and, using the Image Calculator tool, a third image was generated showing those pixels which were positive in both input channels. Using the Particle Analysis tool, the size and number of the thresholded clusters was analysed. Microsoft Excel was used to calculate the fraction of MtDsRed-positive SYN-GFP clusters. GraphPad Prism was used to calculate t-tests and to visualise bar charts.

For each LTP recording, fEPSP amplitude after LTP induction were normalised to the amplitude measured during 10 min recorded baseline. The overall change in amplitude for n recordings from individual slices (from at least 3 animals) was determined by averaging normalised amplitudes, then expressed as a percentage.

Statistics

For optical data, paired t-test was used to calculate statistical significance, whereby terminals with and without mitochondria within the same axon were compared. Unpaired t-test was used to compare neurons from control and MCU$^{+/-}$ animals. Error bars represent SEM. Extra sum-of-squares F test was used to compare time constant (τ) of SV endocytosis between control and MCU$^{+/-}$ neurons. For each LTP recording, fEPSP amplitude was normalized to the amplitude measured 10-15 min before HFS. The overall change in amplitude for n recorded neurons was determined by averaging normalised amplitudes, then expressed as a percentage. For PPR measurements, the average of 5 responses was taken for each interval for each slice. PPR was determined by dividing the peak amplitude of fEPSP2 by that of fEPSP1 using variable inter-stimulus intervals (20–200 ms). Unless otherwise noted, we routinely applied an unpaired t-test to test the difference between the sampled means (Gaussian data scatter). Data were considered significant if $P < 0.05$. Values are given as mean ± SEM. Error bars represent SEM.

Acknowledgements

Competing Interests

The authors declare no competing interests.

References

Ashrafi G, Juan-Sanz J de, Farrell RJ, Ryan TA. 2020. Molecular Tuning of the Axonal Mitochondrial Ca2+ Uniporter Ensures Metabolic Flexibility of Neurotransmission. *Neuron* 105:678-687.e5. doi:10.1016/j.neuron.2019.11.020

Awabdh SA, Gupta-Agarwal S, Sheehan DF, Muir J, Norkett R, Twelvetrees AE, Griffin LD, Kittler JT. 2016. Neuronal activity mediated regulation of glutamate transporter GLT- 1 surface diffusion in rat astrocytes in dissociated and slice cultures. *Glia* 64:1252–1264. doi:10.1002/glia.22997

Bai L, Hof PR, Standaert DG, Xing Y, Nelson SE, Young AB, Magnusson KR. 2004. Changes in the expression of the NR2B subunit during aging in macaque monkeys. *Neurobiol Aging* 25:201–208. doi:10.1016/s0197-4580(03)00091-5

Baughman JM, Perocchi F, Girgis HS, Plovanich M, Belcher-Timme CA, Sancak Y, Bao XR, Strittmatter L, Goldberger O, Bogorad RL, Koteliansky V, Mootha VK. 2011. Integrative genomics identifies MCU as an essential component of the mitochondrial calcium uniporter. *Nature* 476:341–345. doi:10.1038/nature10234

Billups B, Forsythe ID. 2002. Presynaptic mitochondrial calcium sequestration influences transmission at mammalian central synapses. *Journal of Neuroscience* 22:5840–5847.

Bliss T, Lømo T. 1973. Long- lasting potentiation of synaptic transmission in the dentate area of the anaesthetized rabbit following stimulation of the perforant path. *The Journal of physiology* 232:331–356. doi:10.1113/jphysiol.1973.sp010273

Cao X, Cui Z, Feng R, Tang Y, Qin Z, Mei B, Tsien JZ. 2007. Maintenance of superior learning and memory function in NR2B transgenic mice during ageing. *Eur J Neurosci* 25:1815–1822. doi:10.1111/j.1460-9568.2007.05431.x

Chang KT, Niescier RF, Min K-T. 2011. Mitochondrial matrix Ca2+ as an intrinsic signal regulating mitochondrial motility in axons. *Proceedings of the National Academy of Sciences* 108:15456–15461. doi:10.1073/pnas.1106862108

Devine MJ, Kittler JT. 2018. Mitochondria at the neuronal presynapse in health and disease. *Nature Reviews Neuroscience* 19:63–80. doi:10.1038/nrn.2017.170

Divakaruni SS, Dyke AMV, Chandra R, LeGates TA, Contreras M, Dharmasri PA, Higgs HN, Lobo MK, Thompson SM, Blanpied TA. 2018. Long-Term Potentiation Requires a Rapid Burst of Dendritic Mitochondrial Fission during Induction. *Neuron* 100:860-875.e7. doi:10.1016/j.neuron.2018.09.025

Edelstein A, Amodaj N, Hoover K, Vale R, Stuurman N. 2010. Computer control of microscopes using µManager. *Current protocols in molecular biology / edited by Frederick M Ausubel . [et al]* Chapter 14:Unit14.20. doi:10.1002/0471142727.mb1420s92

Jahn R, Fasshauer D. 2012. Molecular machines governing exocytosis of synaptic vesicles. *Nature* 490:201–207. doi:10.1038/nature11320

Kamer KJ, Mootha VK. 2015. The molecular era of the mitochondrial calcium uniporter. *Nature Reviews Molecular Cell Biology* 16:545–553. doi:10.1038/nrm4039

Kamiya H, Shinozaki H, Yamamoto C. 1996. Activation of metabotropic glutamate receptor type 2/3 suppresses transmission at rat hippocampal mossy fibre synapses. *The Journal of physiology* 493:447–455. doi:10.1113/jphysiol.1996.sp021395

Katz B, Miledi R. 1968. The role of calcium in neuromuscular facilitation. *The Journal of physiology* 195:481–492. doi:10.1113/jphysiol.1968.sp008469

Kilkenny C, Browne WJ, Cuthill IC, Emerson M, Altman DG. 2010. Improving Bioscience Research Reporting: The ARRIVE Guidelines for Reporting Animal Research. *PLoS Biology* 8:e1000412. doi:10.1371/journal.pbio.1000412

Kim M-H, Korogod N, Schneggenburger R, Ho W-K, Lee S-H. 2005. Interplay between Na+/Ca2+ exchangers and mitochondria in Ca2+ clearance at the calyx of Held. *Journal of Neuroscience* 25:6057–6065. doi:10.1523/jneurosci.0454-05.2005

Kirichok Y, Krapivinsky G, Clapham DE. 2004. The mitochondrial calcium uniporter is a highly selective ion channel. *Nature* 427:360–364. doi:10.1038/nature02246

Kwon S-K, Scheiffele P, III RS, Lewis TL, Hirabayashi Y, Maximov A, Polleux F. 2016. LKB1 Regulates Mitochondria-Dependent Presynaptic Calcium Clearance and Neurotransmitter Release Properties at Excitatory Synapses along Cortical Axons. *PLoS Biology* 14:e1002516. doi:10.1371/journal.pbio.1002516

Lassalle J-M, Bataille T, Halley H. 2000. Reversible Inactivation of the Hippocampal Mossy Fiber Synapses in Mice Impairs Spatial Learning, but neither Consolidation nor Memory Retrieval, in the Morris Navigation Task. *Neurobiol Learn Mem* 73:243–257. doi:10.1006/nlme.1999.3931

Law AJ, Weickert CS, Webster MJ, Herman MM, Kleinman JE, Harrison PJ. 2003. Expression of NMDA receptor NR1, NR2A and NR2B subunit mRNAs during development of the human hippocampal formation. *Eur J Neurosci* 18:1197–1205. doi:10.1046/j.1460-9568.2003.02850.x

Lee D, Lee K-H, Ho W-K, Lee S-H. 2007. Target Cell-Specific Involvement of Presynaptic Mitochondria in Post-Tetanic Potentiation at Hippocampal Mossy Fiber Synapses. *J Neurosci* 27:13603–13613. doi:10.1523/jneurosci.3985-07.2007

Marland JRK, Hasel P, Bonnycastle K, Cousin MA. 2016. Mitochondrial Calcium Uptake Modulates Synaptic Vesicle Endocytosis in Central Nerve Terminals. *Journal of Biological Chemistry* 291:2080–2086. doi:10.1074/jbc.m115.686956

Mink JW, Blumenschine RJ, Adams DB. 1981. Ratio of central nervous system to body metabolism in vertebrates: its constancy and functional basis. *Am J Physiology-regulatory Integr Comp Physiology* 241:R203–R212. doi:10.1152/ajpregu.1981.241.3.r203

Murphy E, Pan X, Nguyen T, Liu J, Holmström KM, Finkel T. 2014. Unresolved questions from the analysis of mice lacking MCU expression. *Biochemical and Biophysical Research Communications* 449:384–385. doi:10.1016/j.bbrc.2014.04.144

Nicoll RA, Schmitz D. 2005. Synaptic plasticity at hippocampal mossy fibre synapses. *Nature Reviews Neuroscience* 6:863–876. doi:10.1038/nrn1786

Otto C, Kovalchuk Y, Wolfer DP, Gass P, Martin M, Zuschratter W, Gröne HJ, Kellendonk C, Tronche F, Maldonado R, Lipp H-P, Konnerth A, Schütz G. 2001. Impairment of Mossy Fiber Long-Term Potentiation and Associative Learning in Pituitary Adenylate Cyclase Activating Polypeptide Type I Receptor-Deficient Mice. *J Neurosci* 21:5520–5527. doi:10.1523/jneurosci.21-15-05520.2001

Oxenoid K, Dong Y, Cao C, Cui T, Sancak Y, Markhard AL, Grabarek Z, Kong L, Liu Z, Ouyang B, Cong Y, Mootha VK, Chou JJ. 2016. Architecture of the mitochondrial calcium uniporter. *Nature* 533:269–273. doi:10.1038/nature17656

Padamsey Z, Katsanevaki D, Dupuy N, Rochefort NL. 2021. Neocortex saves energy by reducing coding precision during food scarcity. *Neuron*. doi:10.1016/j.neuron.2021.10.024

Pan X, Liu J, Nguyen T, Liu C, Sun J, Teng Y, Fergusson MM, Rovira II, Allen M, Springer DA, Aponte AM, Gucek M, Balaban RS, Murphy E, Finkel T. 2013. The physiological role of mitochondrial calcium revealed by mice lacking the mitochondrial calcium uniporter. *Nat Cell Biol* 15:1464–1472. doi:10.1038/ncb2868

Pathak D, Shields LY, Mendelsohn BA, Haddad D, Lin W, Gerencser AA, Kim H, Brand MD, Edwards RH, Nakamura K. 2015. The role of mitochondrially derived ATP in synaptic vesicle recycling. *Journal of Biological Chemistry* 290:22325–22336. doi:10.1074/jbc.m115.656405

Patron M, Raffaello A, Granatiero V, Tosatto A, Merli G, Stefani DD, Wright L, Pallafacchina G, Terrin A, Mammucari C, Rizzuto R. 2013. The Mitochondrial Calcium Uniporter (MCU): Molecular Identity and Physiological Roles*. *J Biol Chem* 288:10750–10758. doi:10.1074/jbc.r112.420752

Rangaraju V, Calloway N, Ryan TA. 2014. Activity-driven local ATP synthesis is required for synaptic function. *Cell* 156:825–835. doi:10.1016/j.cell.2013.12.042

Rollenhagen A, Sätzler K, Rodriguez EP, Jonas P, Frotscher M, Lübke JHR. 2007. Structural Determinants of Transmission at Large Hippocampal Mossy Fiber Synapses. *J Neurosci* 27:10434–10444. doi:10.1523/jneurosci.1946-07.2007

Ruggiero A, Katsenelson M, Slutsky I. 2021. Mitochondria: new players in homeostatic regulation of firing rate set points. *Trends Neurosci* 44:605–618. doi:10.1016/j.tins.2021.03.002

Salin PA, Scanziani M, Malenka RC, Nicoll RA. 1996. Distinct short-term plasticity at two excitatory synapses in the hippocampus. *Proceedings of the National Academy of Sciences of the United States of America* 93:13304–13309. doi:10.1073/pnas.93.23.13304

Shutov LP, Kim M-S, Houlihan PR, Medvedeva YV, Usachev YM. 2013. Mitochondria and plasma membrane Ca2+-ATPase control presynaptic Ca2+ clearance in capsaicin-sensitive rat sensory neurons. *The Journal of physiology* 591:2443–2462. doi:10.1113/jphysiol.2012.249219

Stefani DD, Patron M, Rizzuto R. 2015. Structure and function of the mitochondrial calcium uniporter complex. *Biochimica et Biophysica Acta (BBA) - Molecular Cell Research* 1853:2006–2011. doi:10.1016/j.bbamcr.2015.04.008

Stefani DD, Raffaello A, Teardo E, Szabò I, Rizzuto R. 2011. A forty-kilodalton protein of the inner membrane is the mitochondrial calcium uniporter. *Nature* 476:336–340. doi:10.1038/nature10230

Styr B, Gonen N, Zarhin D, Ruggiero A, Atsmon R, Gazit N, Braun G, Frere S, Vertkin I, Shapira I, Harel M, Heim LR, Katsenelson M, Rechnitz O, Fadila S, Derdikman D, Rubinstein M, Geiger T, Ruppin E, Slutsky I. 2019. Mitochondrial Regulation of the Hippocampal Firing Rate Set Point and Seizure Susceptibility. *Neuron* 102:1009-1024.e8. doi:10.1016/j.neuron.2019.03.045

Tang Y, Zucker RS. 1997. Mitochondrial involvement in post-tetanic potentiation of synaptic transmission. *Neuron* 18:483–491.

Tang Y-P, Shimizu E, Dube GR, Rampon C, Kerchner GA, Zhuo M, Liu G, Tsien JZ. 1999. Genetic enhancement of learning and memory in mice. *Nature* 401:63–69. doi:10.1038/43432

Tantama M, Martínez-François JR, Mongeon R, Yellen G. 2013. Imaging energy status in live cells with a fluorescent biosensor of the intracellular ATP-to-ADP ratio. *Nature Communications* 4. doi:10.1038/ncomms3550

Vaccaro V, Devine MJ, Higgs NF, Kittler JT. 2017. Miro1-dependent mitochondrial positioning drives the rescaling of presynaptic Ca2+ signals during homeostatic plasticity. *EMBO reports* 18:231–240. doi:10.15252/embr.201642710
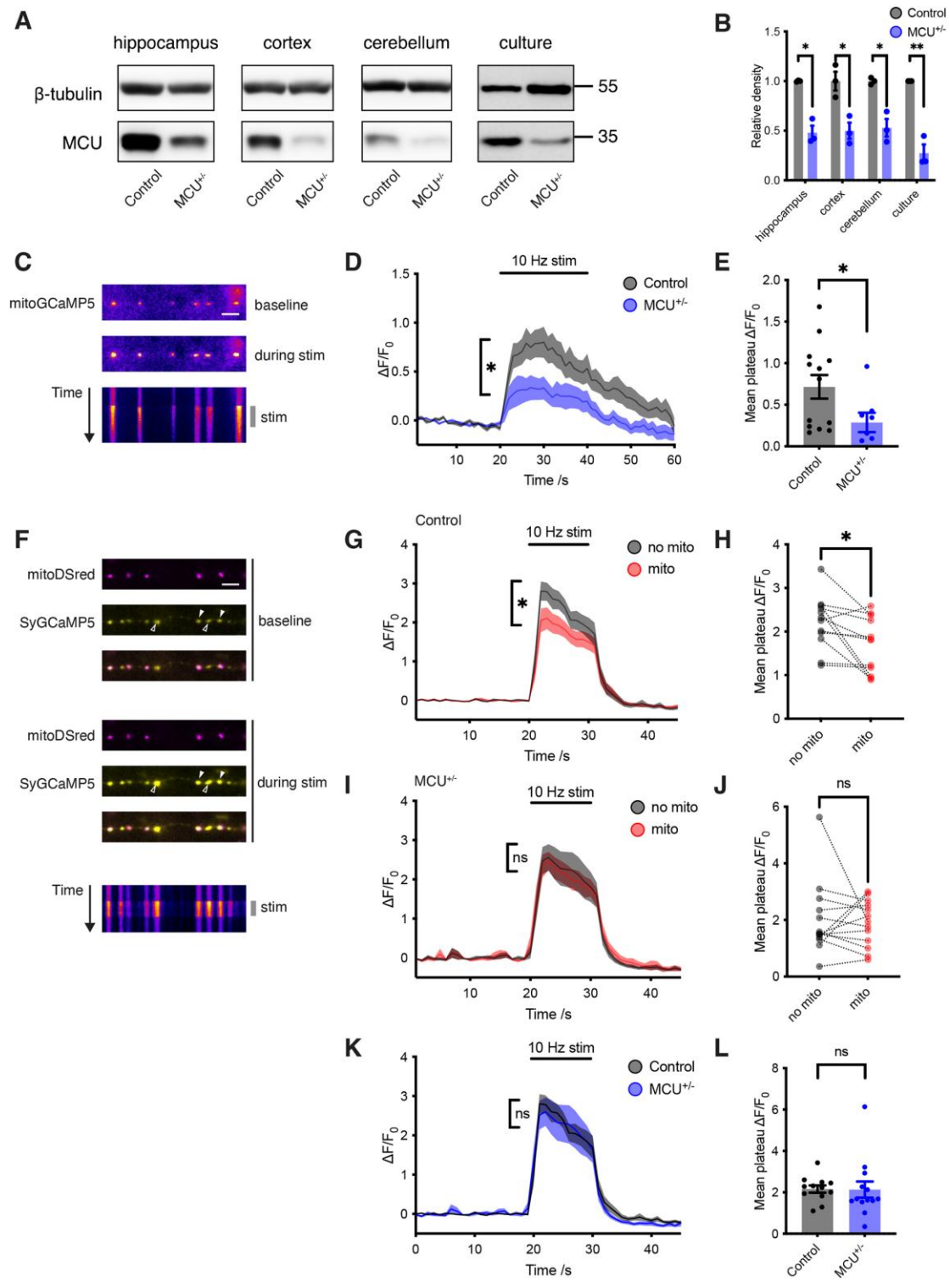
Figures

Fig. 1. MCU heterozygosity blocks mitochondrial presynaptic Ca^{2+} clearance.

a, Western blot of MCU protein in lysate from 6 month old mice (hippocampus, cortex and cerebellum), and E16 primary neuronal cultures.

b, Quantification of MCU protein level, normalised to β-tubulin (unpaired t-tests, n = 3). Hippocampus, *P = 0.002; cortex, *P = 0.016; cerebellum, *P = 0.007; primary neuronal cultures, **P = 0.001.

c, Live images of neurons transfected with mitoGCaMP5 before and during 10 Hz field stimulation (pseudocolour). Kymograph shows change in fluorescence over time (60 s). Scale bar, 5 μm.

d, Average ΔF/F$_0$ mitoGCaMP5 traces from control neurons (n = 13, grey) and MCU$^{+/-}$ neurons (n = 8, blue) showing average increase in mitochondrial fluorescence following stimulation for 20 s (t = 20—40) at 10 Hz.

e, Average Ca^{2+} rise in mitochondria following stimulation (average of ΔF/F$_0$ measurements taken for Δt = 20—40 s from **d**). ΔF/F$_0$ for mitochondria from control neurons = 0.7 ± 0.14 (n = 13), and for mitochondria from MCU$^{+/-}$ neurons = 0.3 ± 0.12 (n = 8) (unpaired t-test, *P = 0.049).

f, Live images of neurons transfected with mitoDSred (magenta) and SyGCaMP5 (yellow) before and during 10 Hz field stimulation. Kymograph shows change in fluorescence of SyGCaMP5 over time. Filled arrowheads indicate terminals occupied by mitochondria, and empty arrowheads indicate unoccupied terminals.

g, Average ΔF/F$_0$ SyGCaMP5 traces from control neurons (n = 12) plotting average of terminals without mitochondria (grey) and with mitochondria (red). Stimulation occurred for 10 s (t = 20—40) at 10 Hz.

h, Average Ca^{2+} response following stimulation of control neurons, comparing terminals with and without a mitochondrion (average of ΔF/F$_0$ measurements taken for Δt = 20—30 s from **g**). ΔF/F$_0$ = 1.7 ± 0.18 in terminals with mitochondria, and 2.2 ± 0.17 in terminals without mitochondria (n = 12) (paired t-test, *P = 0.016).

i, Average ΔF/F$_0$ SyGCaMP5 traces from MCU$^{+/-}$ neurons (n = 13) plotting average of terminals without mitochondria (grey) and with mitochondria (red). Stimulation occurred for 10 s (t = 20—40) at 10 Hz.

j, Average Ca^{2+} response following stimulation of MCU$^{+/-}$ neurons, comparing terminals with and without mitochondria (average of ΔF/F$_0$ measurements taken for Δt = 20—30 s from **g**). ΔF/F$_0$ = 1.9 ± 0.18 in terminals with mitochondria, and 2.0 ± 0.18 in terminals without mitochondria (n = 13) (paired t-test, P = 0.83).

k, Average ΔF/F$_0$ SyGCaMP5 traces in terminals without mitochondria, in control (n = 12, grey) and MCU$^{+/-}$ neurons (n = 13, blue). Stimulation occurred for 10 s (t = 20—40) at 10 Hz.

l, Average Ca^{2+} response following stimulation of control and $MCU^{+/-}$ neurons, in terminals without mitochondria (average of $\Delta F/F_0$ measurements taken for Δt = 20—30 s from **k**). $\Delta F/F_0$ = 2.2 ± 0.17 in terminals from control neurons (n = 12), and 2.1 ± 0.39 in terminals from $MCU^{+/-}$ neurons (n = 13) (unpaired t-test, P = 0.95).

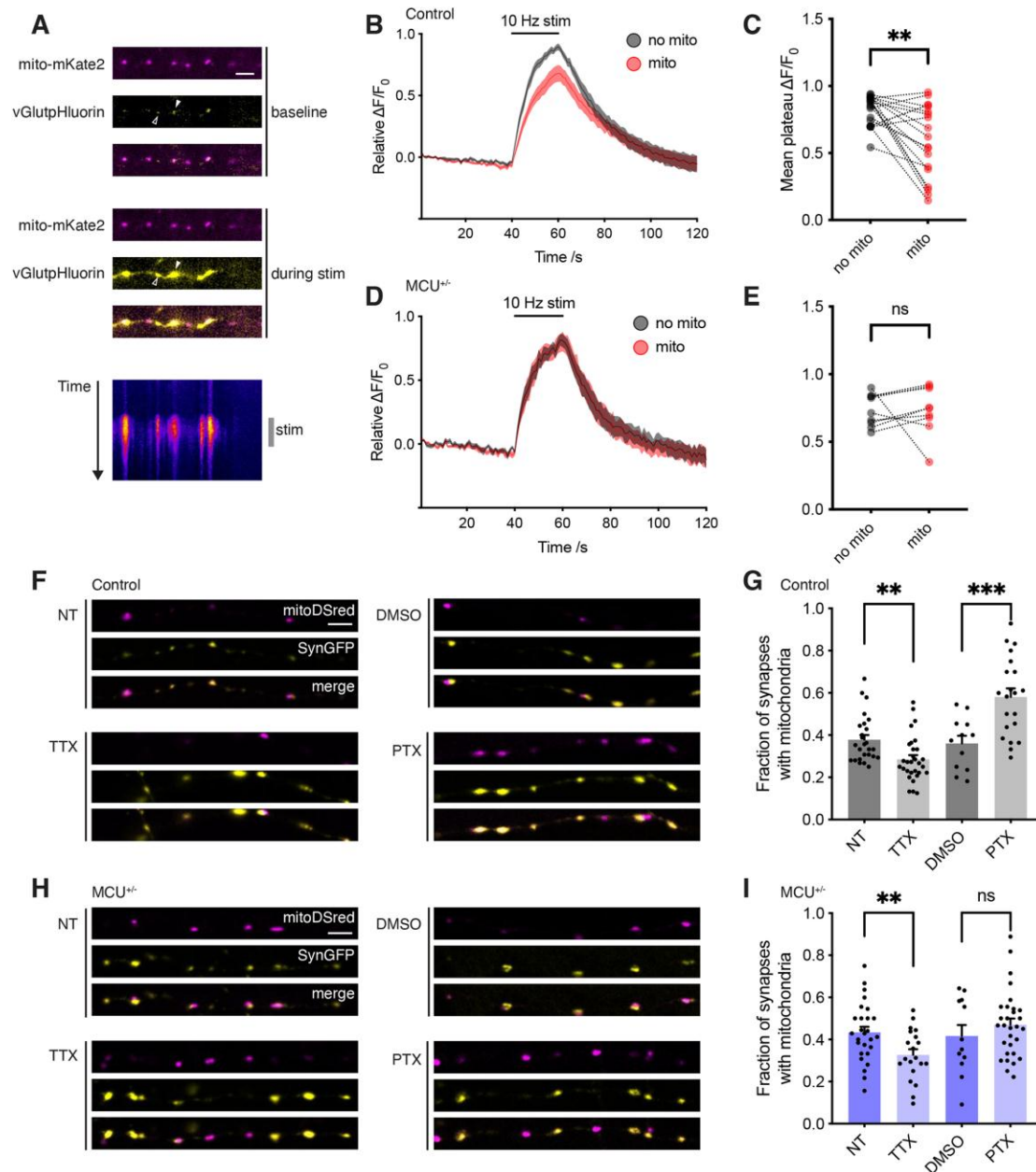Experiments were performed in E16 mouse hippocampal neuronal cultures at DIV 10-12. Error bars represent SEM.

Fig. 2. Functional impact of MCU heterozygosity on synaptic vesicle fusion and activity-dependent redistribution of mitochondria.

a, Live images of neurons transfected with mito-mKate2 (magenta) and vGlutpHluorin (yellow) before and during 10 Hz field stimulation. Kymograph shows change in fluorescence of vGlutpHluorin over time. Filled arrowhead indicates synaptic terminal occupied by mitochondria, and empty arrowhead indicates an unoccupied terminal.

b, Average $\Delta F/F_0$ vGlutpHluorin traces from control neurons (n = 19) plotting average of terminals without mitochondria (grey trace) and with mitochondria (red trace). Stimulation occurred for 20 s (t = 40—60) at 10 Hz.

c, Average mean vGlutpHluorin response following stimulation of control neurons (average of $\Delta F/F_0$ measurements taken for Δt = 50—60 s from **b**). $\Delta F/F_0$ = 0.59 ± 0.06 in terminals with mitochondria, and 0.82 ± 0.03 in terminals without mitochondria (n = 19) (paired t-test, **P = 0.003).

d, Average $\Delta F/F_0$ vGlutpHluorin traces from MCU$^{+/-}$ neurons (n = 9) plotting average of terminals without mitochondria (grey) and with mitochondria (red). Stimulation occurred for 20 s (t = 40—60) at 10 Hz.

e, Average mean vGlutpHluorin response following stimulation of MCU$^{+/-}$ neurons (average of $\Delta F/F_0$ measurements taken for Δt = 50—60 s from **d**). $\Delta F/F_0$ = 0.73 ± 0.04 in terminals with mitochondria, and 0.73 ± 0.06 in terminals without mitochondria (n = 9) (paired t-test, P = 0.99).

f, Confocal images of fixed control neurons transfected with mitoDSred (magenta) and SynGFP (yellow). Neurons are either non-treated (NT), TTX-treated (1 µM, 48 h), DMSO-treated (1:2000, 48 h) or PTX-treated (100 µM, 48 h). Scale bar, 5 µm.

g, Fraction of SynGFP clusters co-localising with mitochondria in control neurons. NT 0.38 ± 0.02 (n = 26), TTX 0.29 ± 0.02 (n = 30) (unpaired t-test, **P = 0.002). DMSO 0.36 ± 0.04 (n = 12), PTX 0.58 ± 0.04 (n = 21) (unpaired t-test, ***P = 0.001).

h, Confocal images of neuronal processes of fixed MCU$^{+/-}$ neurons transfected with mitoDSred (magenta) and SynGFP (yellow), with the same conditions as **f**.

i, Fraction of SynGFP clusters co-localising with mitochondria in MCU$^{+/-}$ neurons. NT 0.43 ± 0.03 (n = 27), TTX 0.33 ± 0.03 (n = 20) (unpaired t-test, P = 0.35). DMSO 0.42 ± 0.05 (n = 12), PTX 0.47 ± 0.03 (n = 30) (unpaired t-test, **P = 0.008).

Experiments were performed in E16 mouse hippocampal neuronal cultures at DIV 10-12. Error bars represent SEM.
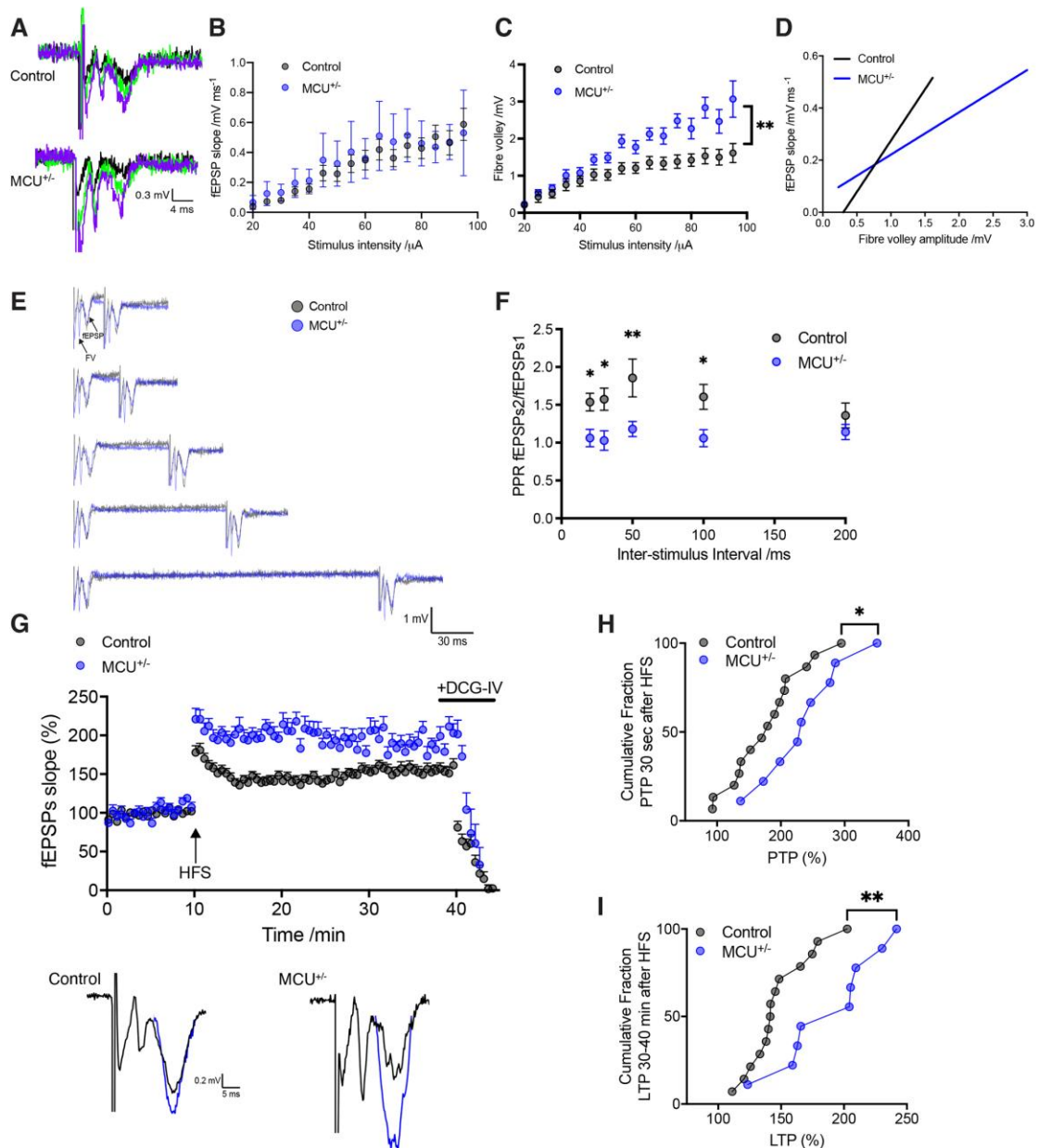
Fig. 3. Larger fibre volley amplitude, loss of paired-pulse facilitation and increased PTP and LTP at DG-CA3 mossy fibre synapse in MCU$^{+/-}$ hippocampal slices.

a, Representative traces of DG-CA3 mossy fibre fEPSPs are shown for control (top) and MCU$^{+/-}$ (bottom). The responses to a range of different stimulus intensities (30-80 μA) are superimposed.

b, Input-output relation for control (black circles) and MCU$^{+/-}$ (blue circles) showing no difference in basal transmission (Control n = 13 slices; MCU$^{+/-}$ n = 10 slices; two-way ANOVA, P = 0.45).

c, Input-output relation for fibre volleys showing higher fibre volley amplitudes in MCU$^{+/-}$ (Control n = 13 slices; MCU$^{+/-}$ n = 10 slices; two-way-ANOVA, **P = 0.01).

d, Mossy fibre fEPSP slope plotted against fibre volley amplitude for the same data (linear regression analysis, two-way-ANOVA, ****P < 0.0001).

e, Examples of PPR in control neurons (grey) and MCU$^{+/-}$ (blue) for a range of inter-stimulus intervals.

f, Mean PPR was reduced at inter-stimulus intervals of between 20 - 100ms in MCU$^{+/-}$ mouse (Control n = 12 slices; MCU$^{+/-}$ n = 12 slices). Unpaired non-parametric Mann-Whitney test: 20 ms *P = 0.0188, 30 ms *P = 0.0112, 50 ms **P = 0.0015, 100 ms *P = 0.03, 200 ms P = 0.4562.

g, Normalised fEPSP slope measurements for control (black circles) and MCU$^{+/-}$ (blue circles) before and after LTP induction (arrow). Representative traces of fEPSPs before (black) and after LTP induction (blue) from control (left) and MCU$^{+/-}$ (right) shown below.

h, Cumulative fraction of PTP showing a shift towards higher values in MCU$^{+/-}$ slices for the first 3 minutes after LTP induction (control 178.5 ± 14.88%, MCU$^{+/-}$ 236.3 ± 21.32%, n = 9 - 15, unpaired t-test, *P = 0.0323).

i, Cumulative fraction of LTP 30-40 minutes after HFS train showing a shift towards higher LTP% in MCU$^{+/-}$ slices (control 147.6 ± 6.65%, MCU$^{+/-}$ 189.2 ± 12.83%, n = 9 - 14, unpaired t-test, **P = 0.0048).

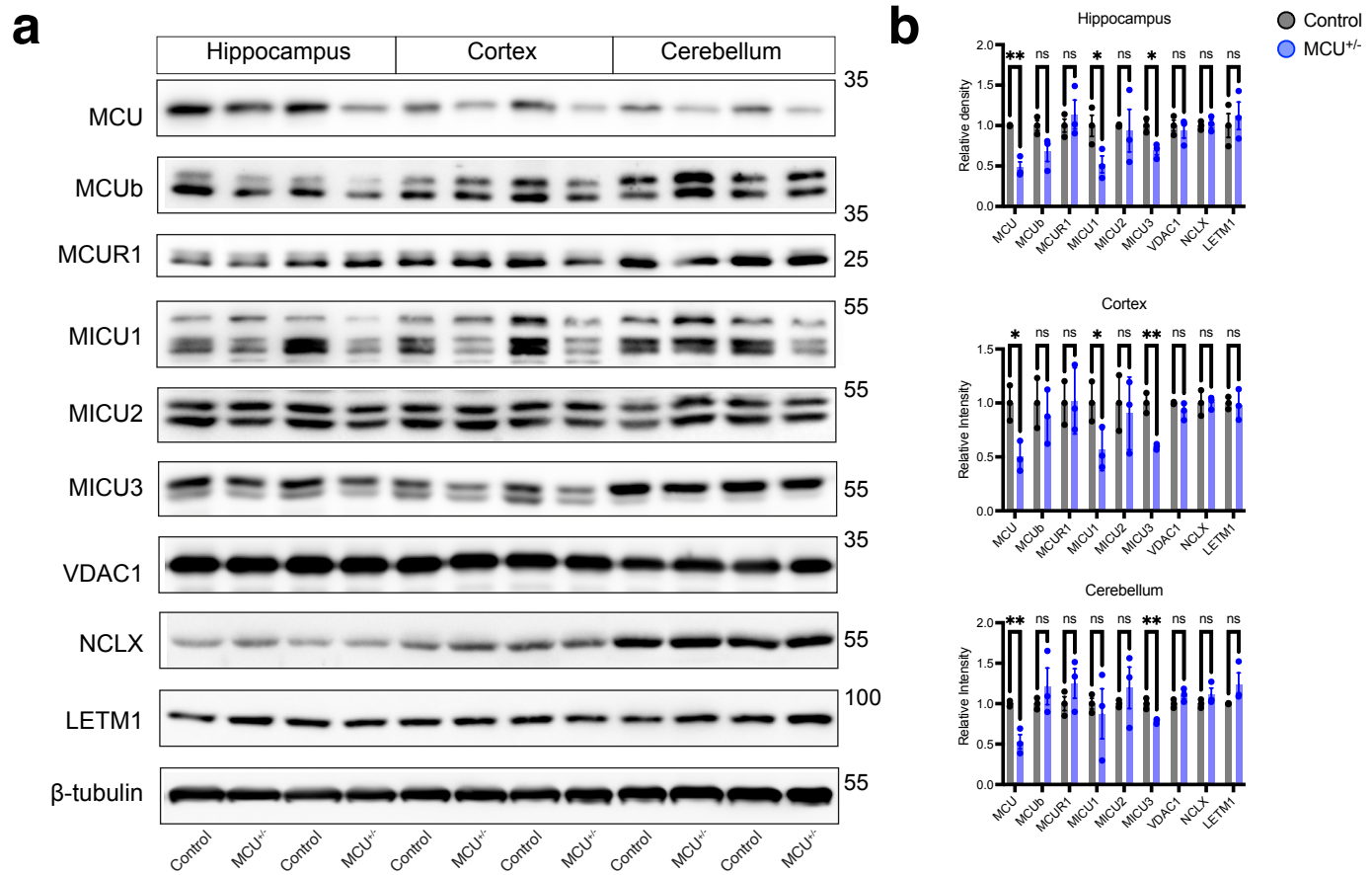Experiments were performed in acute hippocampal slices from mice at 1.5-2 months of age. Error bars represent SEM.

Fig. S1. Mitochondrial Ca^{2+} uptake protein levels in MCU$^{+/-}$ animals.

a, Western blot for mitochondrial Ca^{2+} uptake proteins in lysate from 6 month old mice (hippocampus, cortex and cerebellum).

b, Quantification of protein level, normalised to β-tubulin.

Hippocampus, $n = 3$, unpaired t-tests: MCUb $P = 0.07$, MCUR1 $P = 0.53$, MICU1 *$P = 0.046$, MICU2 $P = 0.83$, MICU3 *$P = 0.01$, VDAC1 $P = 0.64$, NCLX $P = 0.74$, LETM1 $P = 0.62$.

Cortex, $n = 3$, unpaired t-tests: MCUb $P = 0.56$, MCUR1 $P = 0.93$, MICU1 *$P = 0.044$, MICU2 $P = 0.71$, MICU3 **$P = 0.001$, VDAC1 $P = 0.16$, NCLX $P = 0.97$, LETM1 $P = 0.85$.

Cerebellum, $n = 3$, unpaired t-tests: MCUb $P = 0.40$, MCUR1 $P = 0.28$, MICU1 $P = 0.71$, MICU2 $P = 0.49$, MICU3 **$P = 0.007$, VDAC1 $P = 0.13$, NCLX $P = 0.25$, LETM1 $P = 0.16$.
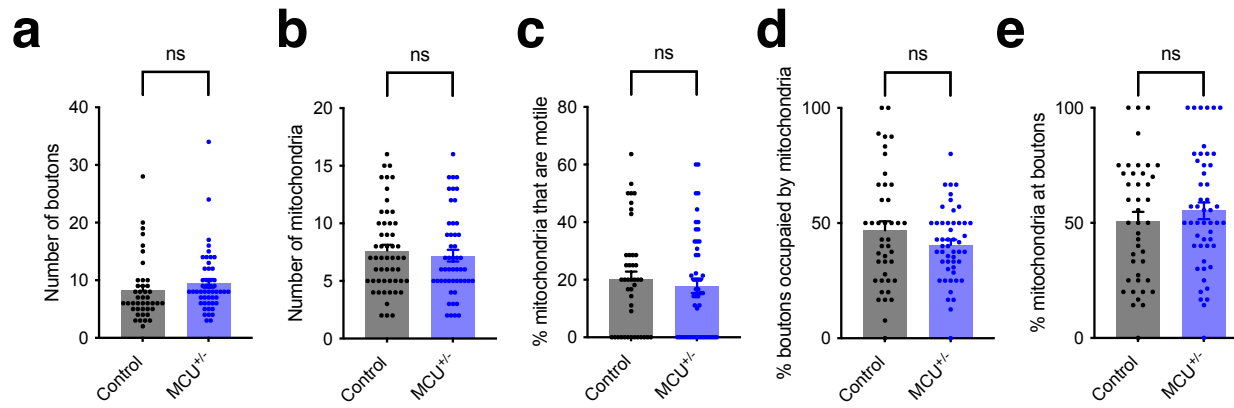
Fig. S2. Characterisation of individual neurons from MCU⁺ᐟ⁻ and control cultures.

a, Number of boutons in control and MCU⁺ᐟ⁻ neurons: 8.2 ± 0.83 and 9.5 ± 0.76 respectively, n = 42-50 neurons, unpaired t-test, P = 0.26.

b, Number of mitochondria in control and MCU⁺ᐟ⁻ neurons: 7.6 ± 0.50 and 7.2 ± 0.51 respectively, n = 42-50 neurons, unpaired t-test, P = 0.54.

c, Percentage of motile mitochondria in control and MCU⁺ᐟ⁻ neurons: 20 ± 2.8 and 18 ± 2.5 respectively, n = 42-50 neurons, unpaired t-test, P = 0.56.

d, Percentage of boutons occupied by mitochondria in control and MCU⁺ᐟ⁻ neurons: 47 ± 3.9 and 41 ± 2.2 respectively, n = 42-50 neurons, unpaired t-test, P = 0.39.

e, Percentage of mitochondria at boutons in control and MCU⁺ᐟ⁻ neurons: 51 ± 4.0 and 55 ± 3.6 respectively, n = 42-50 neurons, unpaired t-test, P = 0.41.

Experiments were performed in E16 mouse hippocampal neuronal cultures at DIV 10-12. Error bars represent SEM.
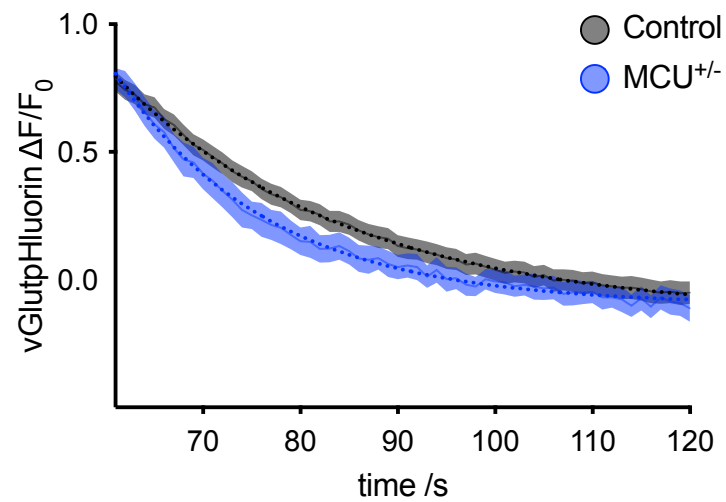
Fig. S3. MCU heterozygosity accelerates synaptic vesicle endocytosis.

Average vGlutpHluorin τ shown by dotted lines for control (grey) and MCU^{+/-} neurons (blue). MCU^{+/-} τ = 15.72s (95% CI 13.6 to 18.39), n = 18 neurons; Control τ = 23.95s (95% CI 20.72 to 28.18), n = 36 neurons). F statistic 13.11 (***P = 0.0003).
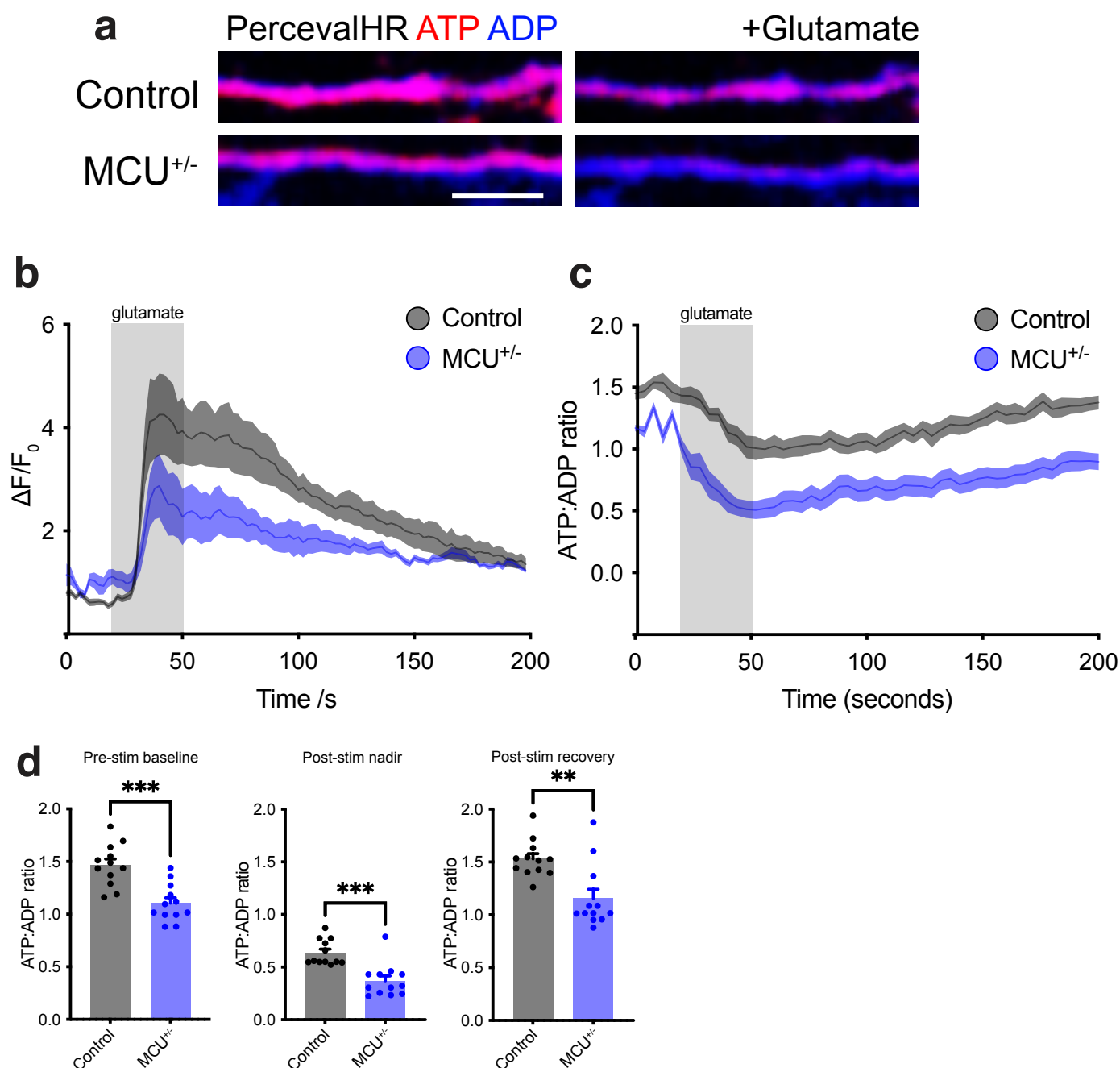
Fig. S4. ATP availability is reduced in MCU⁺ᐟ⁻ neurons.

a, Live images of neurons transfected with PercevalHR before and during glutamate stimulation, shown in false colour. Scale bar, 10 µm.

b, Average $\Delta F/F_0$ MitoGCaMP5 traces from control neurons ($n = 12$, grey) and MCU⁺ᐟ⁻ neurons ($n = 12$, blue). Stimulation with glutamate occurred for 30 s ($t = 20-50$).

c, Average ATP:ADP ratio (derived from PercevalHR imaging) from control neurons ($n = 12$, grey) and MCU⁺ᐟ⁻ neurons ($n = 12$, blue). Stimulation with glutamate occurred for 30 s ($t = 20-50$).

d, Average ATP:ADP ratio (derived from PercevalHR imaging): at baseline prior to glutamate stimulation (Pre-stim baseline), the nadir following glutamate stimulation (Post-stim nadir), and at the end of the imaging period following glutamate stimulation (Post-stim recovery). ATP:ADP ratio was lower in MCU⁺ᐟ⁻ neurons at all three time points. Pre-stim baseline, unpaired t-test, ***$P = 0.0001$. Post-stim nadir, unpaired t-test, ***$P = 0.0001$. Post-stim recovery unpaired t-test, **$P = 0.0013$.
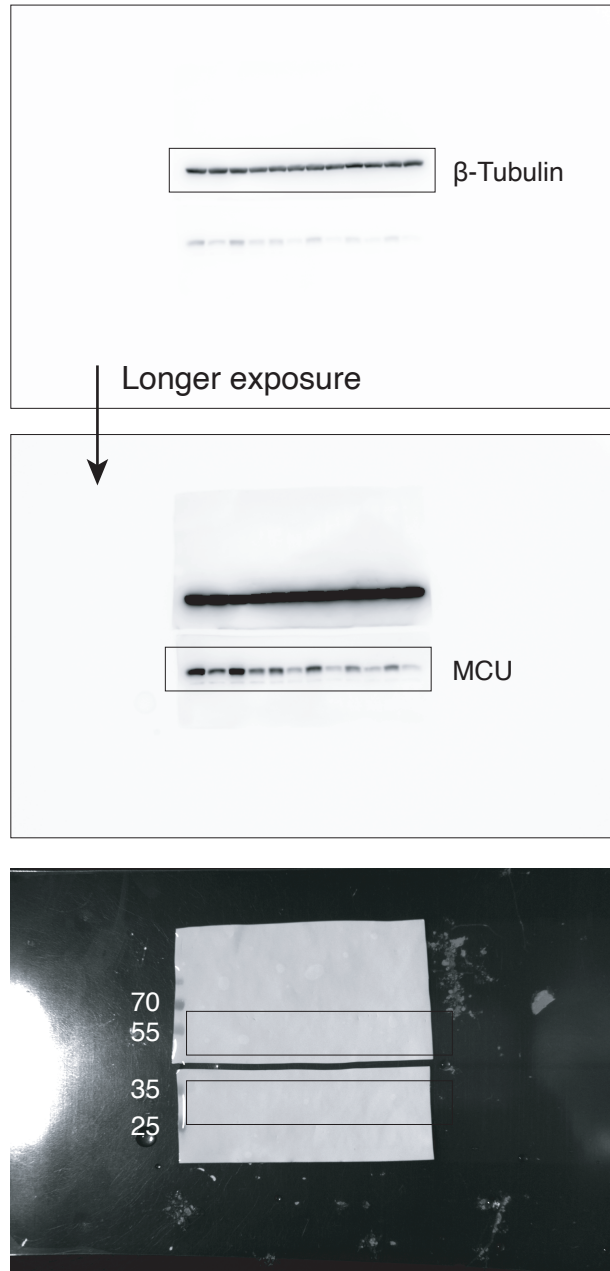
Fig. S5. Blot Transparency related to Figure 1.

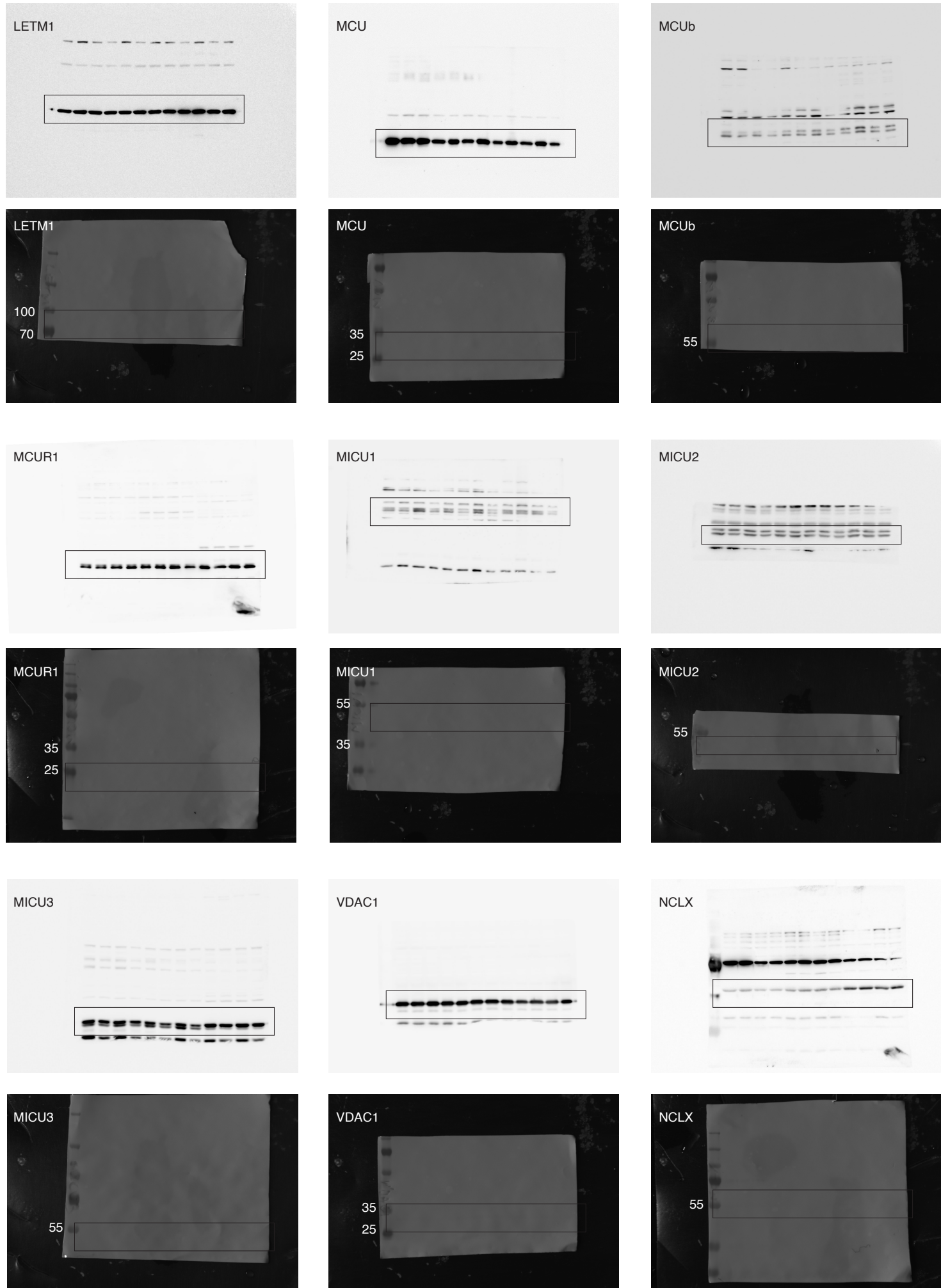*J. Cell Sci.: doi:10.1242/jcs.259823: Supplementary information*

Fig. S6. Blot Transparency related to Supplementary Figure 1.